

www.acsami.org Research Article

Crosslinking of Pressure-Sensitive Adhesives with Polymer-Grafted Nanoparticles

Griffen Desroches, Yuping Wang, Joshua Kubiak, and Robert Macfarlane*



Cite This: ACS Appl. Mater. Interfaces 2022, 14, 9579-9586



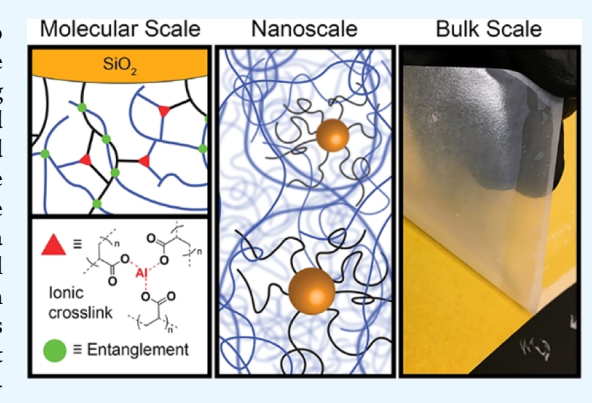
ACCESS

Metrics & More

Article Recommendations

SI Supporting Information

ABSTRACT: Nanocomposite filler particles provide multiple routes to mechanically reinforce pressure-sensitive adhesives (PSAs), as their large surface area to volume ratios provide a means of effectively crosslinking multiple polymer chains. A major advancement could therefore be enabled by the design of a particle architecture that forms multiple physical and chemical interactions with the surrounding polymer matrix, while simultaneously ensuring particle dispersion and preventing particle aggregation. Understanding how such multivalent interactions between a nanoparticle crosslinking point and the PSA polymer affect material mechanical performance would provide both useful scientific knowledge on the mechanical structure—property relationships in polymer composites, as well as a new route to synthesizing useful PSA materials. Herein, we report the use of polymer-grafted nanoparticles (PGNPs) composed of poly(*n*-butyl acrylate-*co*-acrylic acid) chains grafted to SiO₂ nanoparticle (NP)



surfaces to cohesively reinforce PSA films against shear stress without compromising their adhesive properties. The use of acrylic acid-decorated PGNPs allows for ionic crosslinking via metal salt coordination to be used in conjunction with physical entanglement, yielding 33% greater shear resistance and up to 3-fold longer holding times under static load. In addition, the effects of material parameters such as PGNP/crosslinker loading, polymer graft length, and core nanoparticle size on mechanical properties are also explored, providing insights into the use of PGNPs for the rational design of polymer composite-based PSAs.

KEYWORDS: adhesives, nanoparticles, nanocomposite materials, polymer particles, mechanical properties

■ INTRODUCTION

Pressure-sensitive adhesives (PSAs) are a ubiquitous class of material commonly consisting of elastomeric polymers that can rapidly adhere to a substrate under light pressure and with no chemical change to the adhesive itself. The soft, viscoelastic nature of PSAs allows them to flow into and permeate the surface microfeatures of a given substrate, providing a very large interface through which van der Waals forces act to hold the material in place. Furthermore, as the adhesion process does not require any curing or drying steps, PSAs can potentially be removed from substrates without damaging them or leaving undesirable residues. However, because they rely on noncovalent interactions, PSAs are often only useful to a certain service life and maximum load. Both prolonged static load and repeated loading-unloading cycles will cause the PSA film to lose cohesive strength, resulting in degradation and eventual destruction of the adhesive film. Furthermore, PSAs are only useful between the glass transition (T_g) and melting $(T_{\rm m})$ points of the elastomer itself, as temperatures below $T_{\rm g}$ render the material too brittle, and temperatures above T_{m} cause the material to flow and lose adhesion. Crosslinking of the elastomer (such as with acrylic acid (AA) moieties and metal salts) has proven effective at increasing cohesive strength

and extending the functional temperature window, but at the cost of adhesive power.⁴⁻⁶ Alternatively, the addition of the nanoscale filler material (e.g., SiO₂ nanoparticles) improves both substrate adhesion and film cohesion for very low filler content (typically <5 wt %) but ultimately degrades performance as the filler content is further increased, limiting the amount to which they can improve PSA properties. Nanocomposite fillers and surface-modified nanoparticles have more recently emerged as promising candidates for property enhancement, but a great deal of this phase space remains unexplored. 10-13 In particular, these nascent strategies are not amenable to rational ab initio design of filler particle parameters, and their use in conjunction with other reinforcement methods (such as crosslinking and entanglement) is underdeveloped. New nanocomposite filler materials capable of engaging in this type of multimodal reinforcement are

Received: November 26, 2021 Accepted: January 24, 2022 Published: February 11, 2022





Table 1. PGNP Compositional Information

PGNP design	SiO ₂ core diameter (nm)	$\begin{array}{c} P(nBA\text{-co-}AA) \ M_n \\ (g/mol) \end{array}$	$M_{ m w}/M_{ m n}$	nBA/AA molar ratio	σ (chains nm $^{-2}$)	wt % SiO ₂
53 nm SiO ₂ -g-152 kDa P(nBA-co-AA)	53.3 ± 6.6	151,610	2.228	0.951:0.049	0.123	33.049
52 nm SiO ₂ -g-44 kDa P(nBA-co-AA)	51.8 ± 6.0	43,650	1.443	0.942:0.058	0.135	57.509
52 nm SiO ₂ -g-93 kDa P(nBA-co-AA)	51.8 ± 6.0	92,752	1.271	0.944:0.056	0.129	41.923
52 nm SiO ₂ -g-183 kDa P(nBA-co-AA)	51.8 ± 6.0	183,012	1.523	0.943:0.057	0.117	29.541
99 nm SiO ₂ -g-111 kDa P(nBA-co-AA)	99.4 ± 11.1	111,393	1.292	0.942:0.058	0.147	50.180
222 nm SiO ₂ -g-207 kDa P(nBA-co-AA)	222 ± 10.5	107,360	2.224	0.941:0.059	0.082	78.122

therefore a critical need in advancing this area of materials research.

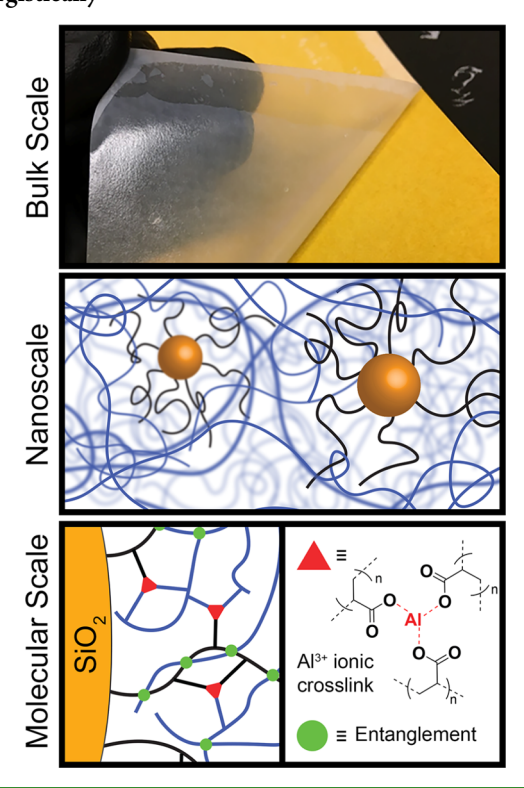
Here, we present a method of using crosslinkable polymergrafted nanoparticles (PGNPs) as functional nanocomposite fillers for acrylate-based PSA films crosslinked via metal coordination. By grafting soft elastomer chains to stiff SiO₂ NP cores, these PGNP additives provide multiple beneficial advancements over bare nanoparticle fillers. Specifically, the polymer brush ensures compatibility of the matrix and filler, preventing aggregation of the particles due to steric repulsion from the polymer brush and ensuring that the overall material is viscoelastic enough to maintain good adhesion. Additionally, the particle acts as a central "node" for the polymer chains grafted to its surface, allowing the entire mass of a polymer brush to act as a collective unit, thereby increasing the multivalency of the interchain interactions (i.e., chain entanglements and metal salt-mediated crosslinking). Thus, the PGNPs can significantly improve the cohesive strength of the film even at low particle concentrations (<5 wt %) without adversely affecting material processability. Moreover, at these low loadings, the number of nanoparticles at the adhesivesubstrate interface remains low and therefore does not affect the material's adhesive strength. The resulting films show significantly improved mechanical performance, leading to 3× longer average active adhesion times prior to failure under a static load. PGNP additives are therefore a powerful tool to improve the utility of pressure-sensitive adhesives.

RESULTS

The PGNPs used in this study consisted of SiO₂ NP cores grafted with an elastomer corona of poly(n-butyl acrylate-co-AA) (poly(nBA-co-AA)) chains, with the AA monomers representing ~6 mol % of the polymer brush. The PGNP architecture allows for multiple methods of reinforcement that should improve material cohesion, including multivalent metalion-mediated crosslinking, polymer chain entanglement, and interfacial slip and chain alignment. By covalently tethering multiple polymer chains at their termini to an inorganic core, the brush architecture gives the PGNPs a greater degree of multivalency in their interactions with the PSA matrix than would be expected for equivalent length free polymer chains. With approximately 10³ to 10⁵ grafted polymer chains per SiO₂ core, individual PGNPs possess a very substantial number of potential crosslinking and entanglement interactions even for relatively small core sizes. A list of PGNP compositions used in this study is given in Table 1, and a graphical representation of their incorporation into PSA films is given in Scheme 1.

The addition of PGNPs should therefore increase the cohesive strength of PSAs that use the same monomer chemistry and binding interactions to increase their adhesive properties and that the amount of this reinforcement could be tuned by both the number of PGNPs in the composite and the

Scheme 1. PGNP-Filled PSA Films as They Appear at the Bulk Scale (Top), Nanoscale (Middle), and Molecular Scale (Bottom); Their Hybrid Core/shell Structure Allows Them to Exploit Multiple Mechanical Enhancement Methods Synergistically



basic design parameters of each PGNP. To test these hypotheses, motorized peel adhesion and static hanging shear measurements were conducted according to tesa and ASTM standard protocols, and the results were compared against control films of either neat polymer or polymer with added silanol-terminated SiO₂ particles. The resulting peel adhesion data (Figure 1, blue and Table S1) show that nanofilled PSA compositions possess small but statistically significant increases in adhesive strength from the polymeronly control films, with the sole exception of the 14.90 ppm film. This finding is consistent with prior literature where small amounts of nanofiller have been shown to beneficially affect peel adhesion,^{7,8} as well as the hypothesis that addition of PGNPs would not negatively impact adhesive behavior.

Cohesive strength (Figure 1, red), on the other hand, was substantially altered by the inclusion of PGNP filler materials. The mean time-tod-failure (TTF) of the PSA specimens concomitantly increased with PGNP content before reaching a maximum of over twofold that of the polymer-only control PSA at 45 ppm PGNPs. The median TTF, on the other hand,

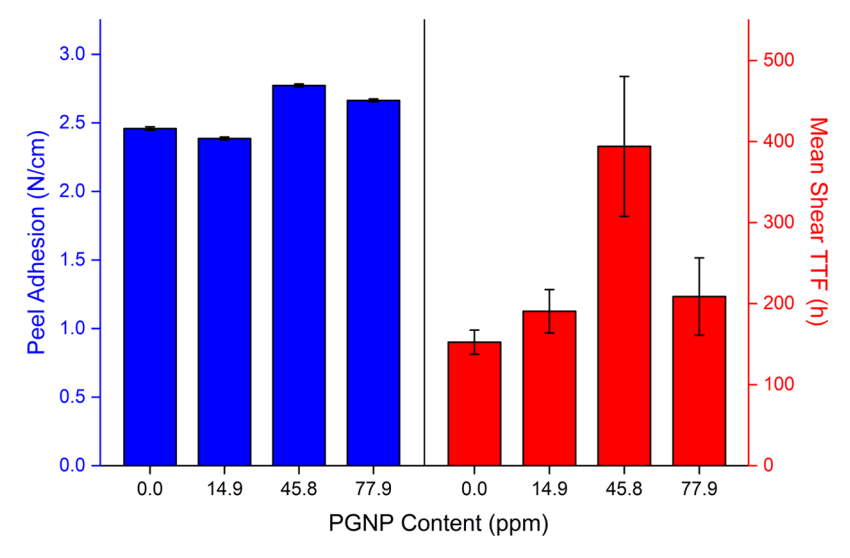


Figure 1. Effect of PGNP content on the peel adhesion (blue) and static shear TTF (red) of nanocomposite PSA films. Both tests made use of PSA films with the 0.2 wt % Al(acac)₃ crosslinker and varying amounts of 53 nm SiO₂/152 kDa P(nBa-co-AA) PGNPs.

showed an even greater increase of nearly threefold over the median failure time of the control film (Table S2). This magnitude of improvement was on par with the best examples of bare nanofiller PSAs reported in the literature. While these data are encouraging for the use of PGNPs as PSA additives to improve performance, the substantial variance between each specimen implied other convoluting factors beyond reasonable control (such as vibration of the building itself potentially affecting the hanging specimens). Thus, dynamic overlap shear testing was employed to gain more insights into compositional trends in stress/strain behavior.

For non-crosslinked PSA films (0 wt % Al(acac)₃, Figure 2 and Table S3) no statistically significant difference was

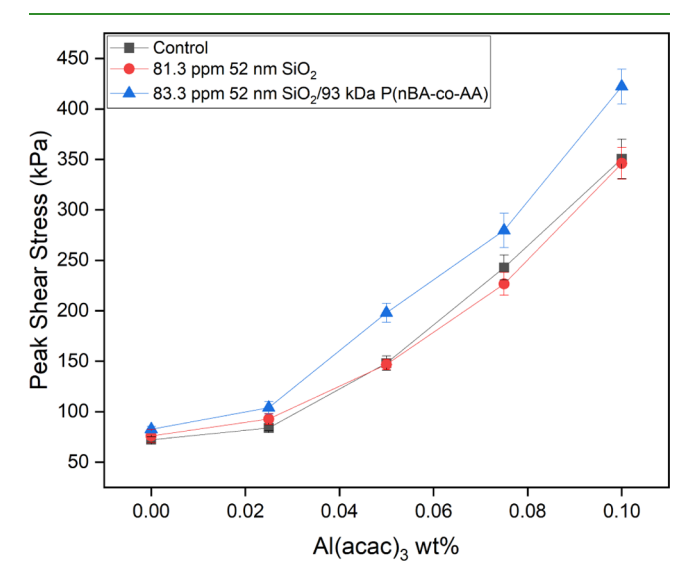


Figure 2. Dynamic overlap shear data for unfilled, bare SiO₂-filled, and PGNP-filled PSA films at varying Al(acac)₃ wt %.

observed between bare SiO₂ NPs and PGNPs for the same nanofiller loading and core size. While uncrosslinked PNGP-filled PSAs exhibited small but significant increases in shear strength over the control PSA, the uncrosslinked SiO₂-filled PSAs did not. With the increasing crosslinker loading, however, the PGNPs exhibited a substantial and statistically significant

improvement in shear resistance over the unfilled control. Furthermore, no statistically significant increase in shear resistance was observed for the bare silica particle control, indicating that the mechanical enhancement derived from PGNPs could not be explained by conventional nanofiller energy dissipation mechanisms as with SiO₂. These data are therefore in agreement with the hypothesis that PGNP multivalency results in greater cohesive strength in the overall film. This hypothesis is further supported by the lack of a consistent trend in fracture energies between the three experimental groups (Figure S1 and Table S4), indicating that the total number of strain-resisting interactions is not changing to any significant degree, but rather that differences in their distribution throughout the matrix must therefore be responsible for the improved shear resistance.

Further testing of the multivalency concept was conducted with a binary mixture of 52 nm bare SiO₂ and ungrafted 110 kDa P(nBa-co-AA) in respective amounts commensurate to the organic/inorganic wt % for the 52 nm/93 kDa PGNPs given in Table 1. The purpose of this additional control was to examine if the mechanical reinforcing effects were due to the brush particle design, as opposed to the addition of particles and lower molecular weight polymers than those that comprised the matrix. In these samples, the concentration of the nanoparticle filler was fixed at ~80 ppm, and both the monomer composition and film wt % of "filler" polymer (both PGNP-grafted and ungrafted) were kept nearly identical. Dynamic overlap shear testing revealed that, for noncrosslinked films, PSAs with the free polymer and bare silica nanofiller exhibited mechanical strengths approximately 15% lower than those of PGNP-filled PSAs (Figure 3, black and Table S5) but were not significantly different from either the control or the SiO₂-filled PSAs. However, in the case of crosslinked PSAs (Figure 3, red), the reduction in strength from the binary nanofiller was significantly more dramatic, falling approximately 35 and 46% below unfilled and PGNPfilled films, respectively.

Having established that the PGNP architecture can indeed improve the cohesive properties of PSAs, the effects of PGNP loading on mechanical properties were examined to determine how the amount of particles affected the overall mechanical

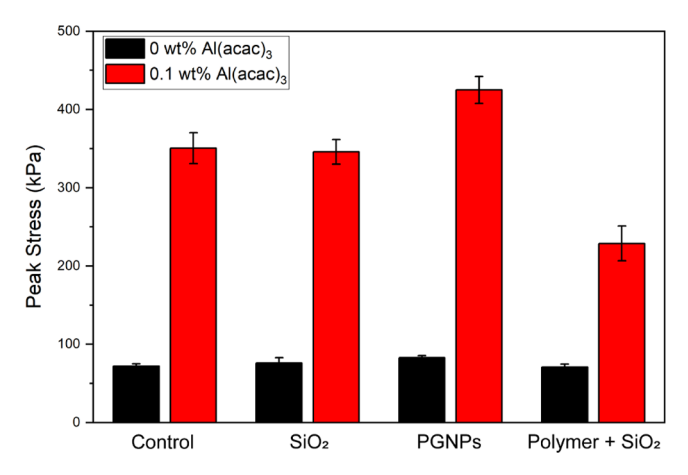


Figure 3. Comparison of dynamic overlap shear strength measurements between PSA films with no nanofiller, 81.3 ppm bare 52 nm SiO_2 , 83.3 ppm 52 nm/93 kDa PGNPs, and a binary mixture of 81.3 ppm 52 nm SiO_2 and a commensurate amount of free 110 kDa ungrafted copolymer.

behavior of the films. For non-crosslinked PSA compositions (Figure 4 and Table S6), bare SiO₂-filled films all differed

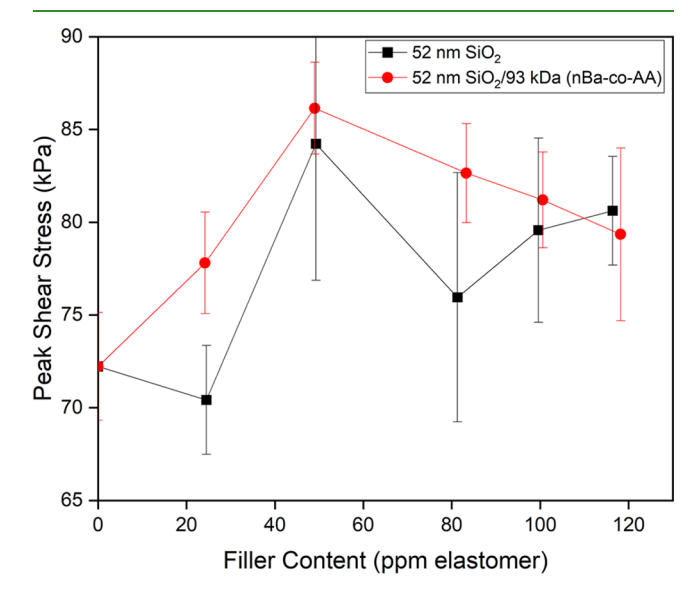


Figure 4. Dynamic overlap shear data for uncrosslinked PSA films containing varying concentrations of bare SiO_2 (black squares) and 52 nm/93 kDa PGNPs (red circles).

significantly in mechanical strength from the control, with the sole exception of the 80 ppm film. PGNP-filled films possessed significantly greater shear strength than the control film at all filler concentrations tested. The general trend observed for both nanofiller types was an increase in shear strength up to 50 ppm filler loading, followed by negative returns with the increasing filler content, while still remaining above the control. This suggests a common mechanism for decline such as aggregation due to chemical incompatibility, consistent with prior investigations on other composite PSAs. 1—9 In these investigations, the agglomerated particles act as significant stress accumulators, 14 thereby weakening PSA shear strength by serving as nucleation sites for cohesive failure. Additionally, unmodified/single-phase nanofillers typically begin aggregating even at very low filler concentrations in PSA systems, ',' which then disperse evenly in the matrix before further

aggregating once a critical nanofiller concentration is reached. Because the mechanical data (Figure 4) closely mirror similar mechanical behavior reported in previous PSA studies,^{7–9,14} we hypothesize that aggregation may also have played a role in the declining mechanical strength with increased filler loading.

Filler content sweeps for highly crosslinked PSA films showed a more exaggerated but otherwise very similar trend (Figure 5), in that both silica- and PGNP-loaded PSA films

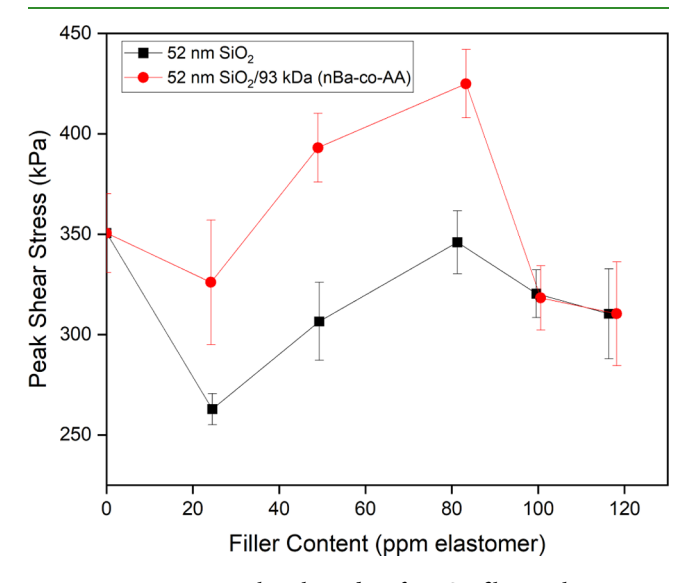


Figure 5. Dynamic overlap shear data for PSA films with 0.1 wt % $Al(acac)_3$ containing varying concentrations of bare SiO_2 (black squares) and 52 nm/93 kDa PGNPs (red circles).

reached an apex at ~ 80 ppm filler loading before declining in mechanical performance. Interestingly, the SiO₂-filled PSAs were significantly weaker under shear than the control film at all filler loadings save for the critical loading of 80 ppm (Figure 5, black, and Table S7). This stands in notable contrast with the uncrosslinked case (Figure 4), where SiO₂ filler particles yielded significant increases in mechanical strength over the control. On the other hand, PGNP filler particles yielded significant increases in mechanical strength up to the critical filler loading, before declining significantly below the control with the additional filler content (Figure 5, red, and Table S7).

It should be noted, however, that the magnitude of the decline beyond 80 ppm was much greater than for noncrosslinked PSAs, which hints at a fundamental loading limit for these nanomaterials in this PSA composition that cannot be overcome with the addition of the crosslinker and may be attributed to the aggregation hypothesis discussed previously. Furthermore, the same initial decrease in mechanical strength for low NP filler content bare SiO₂ PSAs (Figure 5, black) mirrors that of their uncrosslinked counterparts (Figure 4), indicating a similar aggregation behavior even at low filler concentration. Finally, the observed decline in PGNP-filled PSA mechanical strength stands in contrast with the uncrosslinked case (Figure 4), in which PGNP-filled films remained significantly stronger than the control film even beyond the critical filler loading. We hypothesize that the inclusion of the crosslinker may worsen PGNP aggregation beyond the critical concentration, as the PGNPs may preferentially crosslink with each other rather than with the surrounding matrix.

With respect to polymer graft length, it was hypothesized that an increase in graft $M_{\rm n}$ would lead to an increase in shear resistance, albeit with diminishing returns. This trend was predicted because longer polymer grafts enable a greater number of crosslinking residues per individual PGNP, which should both enhance multivalency of crosslinking and allow for more effective chain entanglement to occur. However, longer brush-bound polymer chains can also result in entropic collapse in which they entangle with one another, $^{15-17}$ resulting in lower brush-matrix miscibility as the entangled brush chains push the surrounding matrix away rather than engage in beneficial crosslinking interactions.

For non-crosslinked PSA systems (Figure 6, black line, and Table S8), a marginal increase in shear resistance was indeed

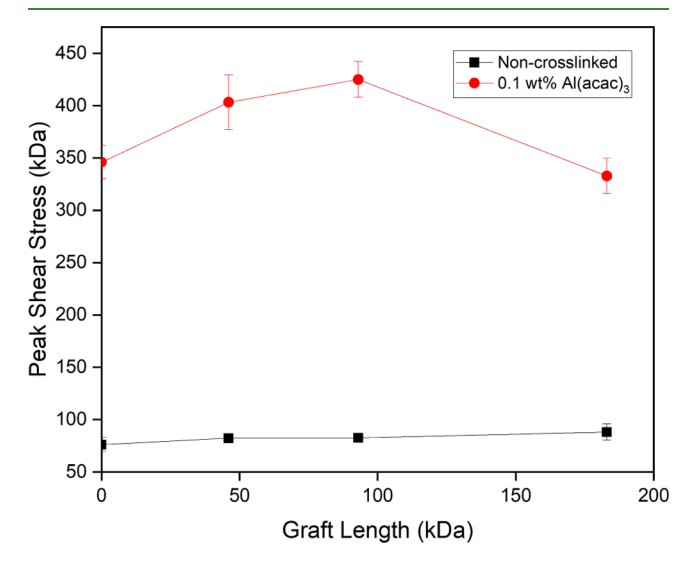


Figure 6. Dynamic overlap shear data for PSA films containing ~80 ppm of the nanofiller with polymer grafts of varying molecular weights. Data are presented for non-crosslinked (black squares) and highly crosslinked (red circles) PSA compositions.

observed with the increasing polymer graft M_n , reaching a maximum at \sim 180 kDa. An analysis of a range of multiple M_n for highly crosslinked PSA films (Figure 6, red line, and Table S8) showed a distinct inflection point at 93 kDa, after which point mechanical performance decreased. It is possible that this inflection point occurs earlier in crosslinked films due to the self-entangled brush crosslinking preferentially with itself rather than with the surrounding elastomer. Consequently, the crosslinked collapsed brush would simply act as a very large filler particle excluding volume from the surrounding elastomer-a discontinuity in the extended crosslinked matrix—and would degrade shear resistance performance in the same way as their bare SiO₂ counterparts. This hypothesis is in agreement with prior computational studies, demonstrated that crosslinking leads to brush collapse/volume contraction and therefore decreased ability to intercalate with the surrounding material. In any event, both data sets are consistent with and support the given hypothesis.

PSA mechanical testing with PGNPs of varying core sizes revealed that larger NP sizes resulted in decreased mechanical strength for all compositions, regardless of the presence of polymer grafts (Figure 7 and Table S9). This was in agreement with the initial hypothesis that smaller nanoparticle cores would yield greater mechanical reinforcement from the

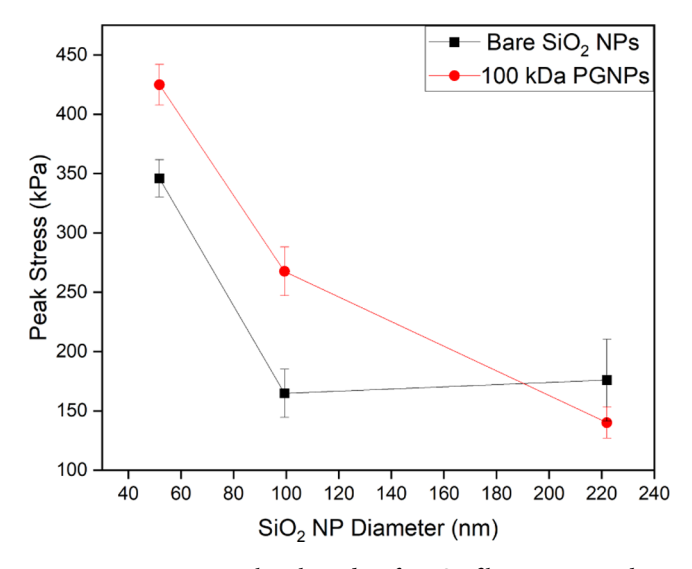


Figure 7. Dynamic overlap shear data for PSA films containing bare SiO_2 and ~ 100 kDa PGNPs with SiO_2 NPs of varying sizes. The fraction SiO_2 in the final film was kept at a constant 1.64 wt %.

resulting PGNPs, which can be attributed to the greater surface curvature of the smaller particles.

Thus, polymer grafts on larger NP cores sit at smaller normal angles relative to each other on the surface than equivalent length chains on smaller NP cores. The reduced surface curvature would therefore keep the brush in a sterically extended configuration, ¹⁹ leading to the same type of brush collapse and loss of mechanical strength as for long-graft PGNPs. This does not, however, explain the decline in mechanical strength for bare SiO₂-filled PSAs. It is therefore hypothesized that the surface area/volume ratio is an important factor as well, in that the mechanical benefit from interfacial slip resistance is offset by the decrease in viscoelasticity/flexural modulus due to the increased size of the nanoparticle fillers. ^{20–22}

CONCLUSIONS

PGNPs have been shown to significantly enhance cohesive strength over control films, as measured by an up to threefold increase in hang time under static load and an up to 33% increase in shear resistance under dynamic load. Some fundamental limits to filler loading and graft length still exist, likely owing to filler aggregation and entropic collapse, respectively, which future researchers may be able to overcome with judicious design of the polymer brush architecture. The ab initio tunability of PGNP design parameters shows a great number of variables and compositions still unexplored as of yet, and further exploration may produce even further improvements and may prove a fruitful subfield in the realm of PSAs. Furthermore, the fact that such significant improvements can be obtained from single-digit weight percents of PGNP fillers bodes well for their potential future use as industrial additives for next-generation adhesives. Future investigations will involve structural manipulations on the nanoscale to determine if nanoscale alignment of PGNP filler materials will have further beneficial effects on adhesive properties.

Scheme 2. Synthetic Scheme for the Preparation of Crosslinkable PGNP Nanocomposite Fillers

EXPERIMENTAL SECTION

Materials. Unless otherwise noted, all reagents were used as received. Triethoxysilane (96%), tetraethoxysilane (99.9%), Tris[2-(dimethylamino)ethyl]amine (Me₆TREN) (99+%), and tin(II) 2ethylhexanoate (95%) were purchased from Alfa Aesar. Ethyl-abromoisobutyrate (EBiB) (98%), 5-hexen-1-ol (98%), acetylacetone (≥99%), Karstedt's catalyst (0.1 M in PDMS), and hydrofluoric acid (aqueous, 48-51 wt %) were purchased from Sigma-Aldrich. The monomers nBA (\geq 99%) and tert-Butyl acrylate (tBA) (98%) were purchased from Sigma-Aldrich and were passed through a column of basic alumina to remove the inhibitor prior to all polymerizations. Anhydrous copper(II) bromide (99+%) was purchased from Acros and stored as a stock solution in dimethylformamide (20 mg/mL). 2-Bromoisobutyryl bromide (>98%) was purchased from TCI America. Ammonium hydroxide (aqueous, 28-30 wt %), triethylamine (99%), and trifluoroacetic acid (TFA) (>97%) were purchased from Thermo Fisher Scientific. The crosslinking agent aluminium(III) acetylacetonate (Al(acac)₃) (99%) was purchased from Sigma-Aldrich and was stored as a stock solution in acetone (3 wt %). All solvents were of analytical grade and were used as received. The adhesive elastomer blend (67 wt % nBA, 30 wt % 2-ethylhexyl acrylate, and 3 wt % AA) and tape backing material (etched PET film and release liner) were provided by industry partners at tesa SE.

Synthesis of Surface-Tetherable ATRP Initiator. The synthesis of BHE was carried out in two separate steps according to previous studies. ^{23–25} In brief, 2-bromoisobutyryl bromide and 5-hexen-1-ol were combined via esterification to form the intermediate 1-(2-bromo-2-methyl)propionyloxy-5-hexene, which was subsequently reacted with triethoxysilane via hydrosilylation to yield (2-bromo-2-methyl)propionyloxyhexyltriethoxysilane (BHE). The initiator was stored in a dark cabinet until active use. See the Supporting Information for full synthetic details.

Synthesis of Silica Nanoparticles with Surface-Tethered ATRP Initiator. Monodisperse SiO_2 NPs were obtained via the Stöber process. Series For a typical reaction aimed at producing ~ 50 nm diameter particles, 200 proof ethanol (1325 mL), ammonia

solution (28 wt %, 81 mL), and nanopure water (36.7 mL) were added to an oven-dried 2 L RB flask with a magnetic stir bar. The solution was heated to 55 °C with a temperature-controlled heating mantle and allowed to equilibrate for 1 h. Tetraethoxysilane (57 mL) was then added quickly under 400 rpm stirring, at which point the stirring was reduced to 150 rpm and the reaction was allowed to proceed for 3 h. The temperature was then reduced to 40 °C and a 10-fold excess of BHE (\sim 16 g) was added incrementally over a 24 h period. The surface-functionalized silica nanoparticles were then recovered by centrifugation after three redispersions each in ethanol and anisole and were stored as a stock solution in anisole for future use. Mean particle diameters and standard deviations were obtained by ImageJ analysis of transmission electron microscopy images taken at MIT MRSEC. SiO₂ nanoparticles with diameters of \sim 50, \sim 100, and \sim 200 nm have been prepared by this method.

Synthesis and Characterisation of Crosslinkable Nanocomposite Brushes. The PGNP brushes used in this study were grown directly from the BHE-functionalized NP surfaces via surface-initiated atom transfer radical polymerization (SI-ATRP). 24,29,30 Due to the known difficulty of polymerizing acidic monomers via ATRP, 31,32 an indirect approach was taken involving copolymerization of nBA and tBA, followed by deprotection to yield AA-containing SiO₂—elastomer nanocomposite particles. This "grafting-from" approach allows for a high degree of both tunability and scalability, and gram-scale synthesis of the nanomaterial was achieved with this method. A full synthetic scheme is given in Scheme 2.

For the preparation of a typical polymer brush batch, BHE-functionalized SiO $_2$ stock solution (4.0000 g/6.4 \times 10^{-6} mol), CuBr $_2$ (0.568 $\mu \rm g/2.54 \times 10^{-6}$ mol), Me $_6 \rm TREN$ (3.4 $\mu \rm L/1.3 \times 10^{-5}$ mol), nBA (7.8 mL/5.4 \times 10^{-2} mol), tBA (0.45 mL/3.1 \times 10^{-3} mol), and anisole (12.55 mL) were added to an oven-dried 25 mL Schlenk flask equipped with a rare-earth stir bar. The reaction mixture was degassed by four cycles of freeze–pump—thaw followed by back-filling with nitrogen gas. A stock solution of tin(II) ethylhexanoate (15.44 mg/mL) in anisole was prepared and degassed by sparging with N $_2$ for 5 min. A 200 $\mu \rm L$ aliquot of this stock solution was then injected into the reaction mixture to activate the reaction (1:3 Cu/Sn), and the flask

was immediately immersed in an 80 °C oil bath and allowed to proceed. Reaction progress was tracked via ¹H NMR. Once the desired conversion had been reached, the reaction was terminated by opening to air and adding oxygenated tetrahydrofuran (THF). The PGNPs were purified by three cycles of centrifugation/redispersion in THF, followed by precipitation in MeOH and drying under vacuum. The as-synthesized PGNP material was soft and tacky to the touch and bore strong resemblance to the bulk adhesive elastomer. Polymer chain molecular weight distribution was assessed with gel-permeation chromatography (GPC), grafting density (σ , chains nm⁻²) of polymer chains on the nanoparticle core surface was determined with thermogravimetric analysis, and copolymer composition was assessed with high-resolution ¹H NMR. Reactivity ratios were calculated based on available literature data, 33 yielding a reactivity product r_1r_2 of 0.994, indicating a near-completely random monomer sequence in the PGNP polymer grafts.

To convert tBA units to AA, deprotection with ~160 equiv TFA was carried out in toluene over 24 h at RT. Deprotected PGNPs were recovered after five cycles of centrifugation/redispersion in THF and stored as a stock solution in THF for later use. Complete deprotection of all *tert*-butyl groups was confirmed by the disappearance of the respective 1.42 ppm peak in the 1 H NMR spectra. PGNPs produced by this method are notably soft and tacky at ambient conditions, very similar to the PSA elastomer blend itself.

Synthesis of Free P(nBa-co-AA). Free polymer chains of the same monomer composition as the PGNPs were synthesized via ARGET-ATRP with similar methods as were used for PGNPs. For a typical free polymer synthesis, a ratio of EBiB/Cu(II)/Me₆TREN/Sn(II)/nBA/tBA of 1:0.35:1.75:1.05:2292:121 along with an equal volume of anisole was added to a 100 mL Schlenk flask. Following the reaction, the polymer was purified by precipitation into cold MeOH 2×, followed by removal of residual monomer under high vacuum at 160 °C. Deprotection of tBA to AA took place in dichloromethane with 160 equiv of TFA at RT for 24 h, at which point the solvent and acid were both removed under reduced pressure. The resulting polymer had a number-averaged molecular weight of M_n = 110,897 g/mol by GPC and a composition of nBa/AA = 0.943:0.057 by NMR.

Preparation of PSA Tape Samples. For a typical reference PSA film with a coating weight of ~50 g m⁻², 2.0 g of tesa elastomer and 8.0 g of toluene were added to a 50 mL RB flask with a rare-earth magnetic stir bar. The mixture was heated to 45 °C and allowed to stir overnight until the elastomer was fully dissolved. The Al(acac)₃ crosslinker (0.0-0.2 wt % relative to dry elastomer) was then added, and the mixture was left to stir for an additional 2 h until fully homogenous. The mixture was then poured out onto release liner and spread to a height of 300 μ m with a doctor blade film applicator. The spread film was then placed in a drying oven preheated to 90 °C to remove solvent for 90 min. Dry films were then crosslinked at 120 °C for 20 min, after which point the oven was switched off and allowed to cool to RT. The etched PET backing material was then applied to the free side of the elastomer film to produce PSA tape reference samples. Double-sided PSA tape samples for dynamic shear testing were prepared by fixing the elastomer to both sides of the PET backer.

Preparation of PGNP-PSA Tape Samples. Films of varying PGNP/tesa elastomer w/w ratios were prepared with a total dry weight of 2.0 g and a total solvent weight of 8.0 g using the same general procedure as for the reference films. Al(acac)₃ crosslinker concentration was measured out relative to the total dry polymeric material (PGNP polymer grafts and free elastomer), not counting the SiO₂ cores. For the purposes of this study, the concentration of PGNPs in the host matrix is given in a molar ratio of parts PGNPs per million parts free elastomer (ppm elastomer).

Static Shear Testing of PSA Tape Samples. PSA tape samples were cut into 6.35 mm wide strips with a double-bladed precision sample cutter and fixed to precleaned stainless steel testing plates. A 2.0 kg steel roller was run back and forth along each tape sample to ensure even contact with the test plate surface. The free ends of the tape strips were then secured to metal fasteners. The samples were then hung from the test-plate end on force-sensitive timers affixed to the wall of the laboratory, and 500 g steel weights were then hung

shock-free from the fastener ends of the tape samples. The samples were then left to cohesively fail under static shear of gravity; upon failure of the sample, the weight would drop free of the test plate, and the timer would stop. Tape samples were tested in triplicate and the median time to failure used as a benchmark for comparing cohesive strength between PSA formulations.

Peel Adhesion Testing of PSA Tape Samples. Peel adhesion testing was carried out with an Imada MX-110 motorized test stand equipped with 180° peel testing fixtures according to ASTM D3330 (method B). Precision specimen cutters were used to cut single-sided PSA tape specimens to uniform width. The specimens were fixed at one end to a motorized actuator/force sensor via film grip attachment and at the other end to a stainless steel stage with a weighted steel roller. Specimens were peeled from the test plate at constant, standardized crosshead speed, and the data were collected as a force over displacement curve with Imada software. The average of each curve was used to calculate average peel adhesion strength and adhesion energy for each tape composition.

Dynamic Shear Testing of PSA Tape Samples. A square 18×18 mm steel punch was used to cut specimens from double-sided PSA samples. The specimens were sandwiched between stainless steel test plates (diagram or picture goes here) and fixed with a screw press under 100 N/cm^2 of pressure for 4 min. Bonded specimens were fixed at one end to the base of the tensile tester, with the free end held by the motorized actuator/force sensor (insert picture or diagram here). The specimens were then subjected to shear stress until failure at a constant crosshead speed of 10 mm/min. Force over displacement data curves were collected with Imada software. A minimum of 10 replicate measurements were taken for each PSA composition to account for variances between individual specimens. Values of mean peak shear stress and associated 99% confidence interval are shown for a variety of compositions.

ASSOCIATED CONTENT

Supporting Information

The Supporting Information is available free of charge at https://pubs.acs.org/doi/10.1021/acsami.1c22997.

Mean peel adhesion strength, SD, 99% confidence intervals, and p-values, static shear TTF triplicate results, fracture energy data, synthesis of (2-Bromo-2-methyl)-propionyloxyhexyltriethoxysilane (BHE) surface-tetherable ATRP initiator, 1H NMR spectra, and TEM images (PDF)

AUTHOR INFORMATION

Corresponding Author

Robert Macfarlane — Department of Materials Science and Engineering, Massachusetts Institute of Technology, Cambridge, Massachusetts 02139, United States; orcid.org/0000-0001-9449-2680; Email: rmacfarl@mit.edu

Authors

Griffen Desroches – Department of Materials Science and Engineering, Massachusetts Institute of Technology, Cambridge, Massachusetts 02139, United States Yuping Wang – Department of Materials Science and

Engineering, Massachusetts Institute of Technology, Cambridge, Massachusetts 02139, United States;
orcid.org/0000-0002-9315-2358

Joshua Kubiak – Department of Materials Science and Engineering, Massachusetts Institute of Technology, Cambridge, Massachusetts 02139, United States

Complete contact information is available at: https://pubs.acs.org/10.1021/acsami.1c22997

Author Contributions

The manuscript was written through contributions of all authors. All authors have given approval to the final version of the manuscript.

Notes

The authors declare no competing financial interest.

ACKNOWLEDGMENTS

This work was funded by tesa GMBH. This work was also supported by an NSF CAREER grant, award no. CHE-1653289, and made use of the MRSEC Shared Experimental Facilities at MIT, supported by the NSF under award no. DMR 14-19807. G.D. would like to acknowledge and thank Perapat P. Gatenil for assistance with material preparation.

REFERENCES

- (1) Benedek, I. Pressure-Sensitive Adhesives and Applications; CRC Press, 2004.
- (2) Benedek, I. Developments In Pressure-Sensitive Products; CRC Press, 2005.
- (3) Benedek, I.; Feldstein, M. M.; Feldstein, M. M. Technology of Pressure-Sensitive Adhesives and Products; CRC Press, 2008.
- (4) Wahdat, H. Influence of Delayed, Ionic Polymer Cross-Linking on Film Formation Kinetics of Waterborne Adhesives. *Macromolecules* **2019**, *15*, 271. accessed June 14, 2021
- (5) Czech, Z. Synthesis and Cross-Linking of Acrylic PSA Systems. *J. Adhes. Sci. Technol.* **2007**, *21*, 625–635.
- (6) Lee, J.-H.; Shim, G.-S.; Kim, H.-J.; Kim, Y. Adhesion Performance and Recovery of Acrylic PSA with Acrylic Elastomer (AE) Blends via Thermal Crosslinking for Application in Flexible Displays. *Polymers* **2019**, *11*, 1959.
- (7) Sardeh Moghadam, R.; Moghbeli, M. R. Effect of Organoclay and Chain-Transfer Agent on Molecular Parameters and Adhesion Performance of Emulsion Pressure-Sensitive Adhesives. *J. Adhes. Sci. Technol.* **2016**, *30*, 284–299.
- (8) Shaikh, S.; Birdi, A.; Qutubuddin, S.; Lakatosh, E.; Baskaran, H. Controlled Release in Transdermal Pressure Sensitive Adhesives Using Organosilicate Nanocomposites. *Ann. Biomed. Eng.* **2007**, *35*, 2130–2137.
- (9) Czech, Z.; Świderska, J. Acrylic Pressure-Sensitive Adhesives Containing SiO Nanoparticles. *Pol. J. Chem. Technol.* **2013**, *15*, 12–14.
- (10) Yamamoto, Y.; Fujii, S.; Shitajima, K.; Fujiwara, K.; Hikasa, S.; Nakamura, Y. Soft Polymer-Silica Nanocomposite Particles as Filler for Pressure-Sensitive Adhesives. *Polymer* **2015**, *70*, *77*–87.
- (11) Fujii, S.; Sawada, S.; Nakayama, S.; Kappl, M.; Ueno, K.; Shitajima, K.; Butt, H.-J.; Nakamura, Y. Pressure-Sensitive Adhesive Powder. *Mater. Horiz.* **2016**, *3*, 47–52.
- (12) Lee, J.-K.; Chin, I.-J. Waterborne Core-Shell Pressure Sensitive Adhesive (PSA) Based on Polymeric Nano-Dispersant. *J. Adhes. Interface* **2016**, *17*, 89–95.
- (13) Wang, T.; Colver, P. J.; Keddie, J. L.; Keddie, L. Soft Polymer and Nano-Clay Supracolloidal Particles in Adhesives: Synergistic Effects on Mechanical Properties. *Soft Matter* **2009**, *5*, 3842–3849.
- (14) Teh, P. L.; Mohd Ishak, Z. A.; Hashim, A. S.; Karger-Kocsis, J.; Ishiaku, U. S. Physical Properties of Natural Rubber/Organoclay Nanocomposites Compatibilized with Epoxidized Natural Rubber. *J. Appl. Polym. Sci.* **2006**, *100*, 1083–1092.
- (15) Martin, J. I.; Wang, Z.-G. Polymer Brushes: Scaling, Compression Forces, Interbrush Penetration, and Solvent Size Effects. *J. Phys. Chem.* **1995**, *99*, 2833–2844.
- (16) Hoy, R. S. Entanglements of an End-Grafted Polymer Brush in a Polymeric Matrix. *Macromolecules* **2007**, *47*, 8389. accessed June 14, 2021
- (17) Meng, D.; Kumar, S. K.; Cheng, S.; Grest, G. S. Simulating the Miscibility of Nanoparticles and Polymer Melts. *Soft Matter* **2013**, *9*, 5417–5427.

- (18) Ozmaian, M.; Jasnow, D.; Eskandari Nasrabad, A.; Zilman, A.; Coalson, R. D. Effects of Cross-Linking on Partitioning of Nanoparticles into a Polymer Brush: Coarse-Grained Simulations Test Simple Approximate Theories. *J. Chem. Phys.* **2018**, *148*, 024902.
- (19) Chen, W.-L.; Cordero, R.; Tran, H.; Ober, C. K. S0th Anniversary Perspective: Polymer Brushes: Novel Surfaces for Future Materials. *Macromolecules* **2017**, *50*, 4089–4113.
- (20) Azimi Dijvejin, Z.; Ghaffarkhah, A.; Sadeghnejad, S.; Vafaie Sefti, M. Effect of Silica Nanoparticle Size on the Mechanical Strength and Wellbore Plugging Performance of SPAM/Chromium (III) Acetate Nanocomposite Gels. *Polym. J.* **2019**, *51*, *693*–707.
- (21) Barghamadi, H.; Atai, M.; Imani, M.; Esfandeh, M. Effects of Nanoparticle Size and Content on Mechanical Properties of Dental Nanocomposites: Experimental versus Modeling. *Iran. Polym. J.* **2015**, 24, 837–848.
- (22) Fu, S.-Y.; Feng, X.-Q.; Lauke, B.; Mai, Y.-W. Effects of Particle Size, Particle/Matrix Interface Adhesion and Particle Loading on Mechanical Properties of Particulate—Polymer Composites. *Composites, Part B* **2008**, *39*, 933–961.
- (23) Kubiak, J. M.; Macfarlane, R. J. Forming Covalent Crosslinks between Polymer-Grafted Nanoparticles as a Route to Highly Filled and Mechanically Robust Nanocomposites. *Adv. Funct. Mater.* **2019**, 29, 1905168.
- (24) Ohno, K.; Morinaga, T.; Koh, K.; Tsujii, Y.; Fukuda, T. Synthesis of Monodisperse Silica Particles Coated with Well-Defined, High-Density Polymer Brushes by Surface-Initiated Atom Transfer Radical Polymerization. *Macromolecules* **2005**, *38*, 2137–2142.
- (25) Yan, J.; Pan, X.; Schmitt, M.; Wang, Z.; Bockstaller, M. R.; Matyjaszewski, K. Enhancing Initiation Efficiency in Metal-Free Surface-Initiated Atom Transfer Radical Polymerization (SI-ATRP). *ACS Macro Lett.* **2016**, *5*, 661–665.
- (26) Stöber, W.; Fink, A.; Bohn, E. Controlled Growth of Monodisperse Silica Spheres in the Micron Size Range. *J. Colloid Interface Sci.* **1968**, *26*, 62–69.
- (27) Lei, X.; Yu, B.; Cong, H.-L.; Tian, C.; Wang, Y.-Z.; Wang, Q.-B.; Liu, C.-K. Synthesis of Monodisperse Silica Microspheres by a Modified Stöber Method. *Integr. Ferroelectr.* **2014**, *154*, 142–146.
- (28) Huang, Y.; Pemberton, J. E. Synthesis of Uniform, Spherical Sub-100nm Silica Particles Using a Conceptual Modification of the Classic LaMer Model. *Colloids Surf.*, A **2010**, 360, 175–183.
- (29) Khabibullin, A.; Mastan, E.; Matyjaszewski, K.; Zhu, S. Surface-Initiated Atom Transfer Radical Polymerization. In *Controlled Radical Polymerization at and from Solid Surfaces*; Vana, P., Ed.; Advances in Polymer Science; Springer International Publishing: Cham, 2016; pp 29–76
- (30) Dong, H. One-Pot Synthesis of Robust Core/Shell Gold Nanoparticles. J. Am. Chem. Soc. 2008, 130, 12852. accessed June 28, 2021)
- (31) Matyjaszewski, K.; Xia, J. Atom Transfer Radical Polymerization. Chem. Rev. 2001, 101, 2921-2990.
- (32) Treat, N. D.; Ayres, N.; Boyes, S. G.; Brittain, W. J. A Facile Route to Poly(Acrylic Acid) Brushes Using Atom Transfer Radical Polymerization. *Macromolecules* **2006**, 39, 26–29.
- (33) Siołek, M.; Matlengiewicz, M. Reactivity Ratios of Butyl Acrylates in Radical Copolymerization with Methacrylates. *Int. J. Polym. Anal. Charact.* **2014**, *19*, 222–233.